Supporting Information for Ultrafast carrier relaxation dynamics in a nodal-line semimetal $PtSn_4$

Tianyun Lin[∞,†] Yongkang Ju[∞,‡] Haoyuan Zhong,[†] Xiangyu Zeng,[¶] Xue Dong,[¶] Changhua Bao,[†] Hongyun Zhang,[†] Tian-Long Xia,[¶] Peizhe Tang,[*,‡,§] and Shuyun Zhou[*,†,‖]

†*State Key Laboratory of Low Dimensional Quantum Physics and Department of Physics, Tsinghua University, Beijing 100084, P.R. China*

‡*School of Materials Science and Engineering, Beihang University, Beijing 100191, P. R. China*

¶*Department of Physics and Beijing Key Laboratory of Opto-electronic Functional Materials and Micro-nano Devices, Renmin University of China, Beijing 100872, P. R. China*

§*Max Planck Institute for the Structure and Dynamics of Matter, Center for Free-Electron Laser Science, 22761 Hamburg, Germany*

‖*Collaborative Innovation Center of Quantum Matter, Beijing 100084, P.R. China*

E-mail: peizhet@buaa.edu.cn; syzhou@mail.tsinghua.edu.cn

Contents:

- **Supporting Note 1: Dirac nodal lines around Z point.**
- **Supporting Note 2: The comparison of the raw data and normalized data.**
- **Supporting Note 3: The relaxation of excited electrons in $PtSn_4$.**
- **Supporting Note 4: The time resolution of the system.**
- **Supporting Note 5: Influence of spin-orbital coupling effect.**

Dirac nodal lines around Z point

To show the evolution of Dirac nodal lines around the Z point, we calculate the 3D bulk band structures near the Fermi level for $PtSn_4$. We find the Dirac nodal lines around the Z point in the Brillouin zone (BZ) of the conventional unit cell are mainly contributed by four bands around the Fermi level. Figure S1a shows the first BZ and the projected surface Brillouin zone (SBZ) for $PtSn_4$ within a conventional unit cell. The Dirac nodal lines are located in the k_y-k_z plane (the yellow shaded area in Figure S1a), which are protected by the C_2 rotational symmetry and the mirror symmetry in $PtSn_4$. In such a momentum plane, we obtain the evolution of crossing points in the Dirac nodal lines as shown in Figure S1b, in which four nodal lines can be identified. Moreover, Figure S1c-g shows the calculated band structures of $PtSn_4$ along the momentum cuts marked in Figure S1b, in which blue lines and red lines stand for the four bands mentioned above. Along the line of ZT (cut 5), all states are doubly degenerated (Figure S1g), thus at the $\pm C$ points (Figure S1b), these crossings are four-fold degenerate. Once the k point is slightly away from $\pm C$, the four-fold crossing points will split as four gapless points in these nodal lines with small energy splitting. Considering the projection of bulk states in 3D BZ to 2D SBZ, bulk gapless points along k_y belonging to different nodal lines will project on the same momentum $\overline{\mathrm{k}}$ point in SBZ. Due to the small energy variation, under the projection, these gapless points overlap with each other and are difficult to distinguish.

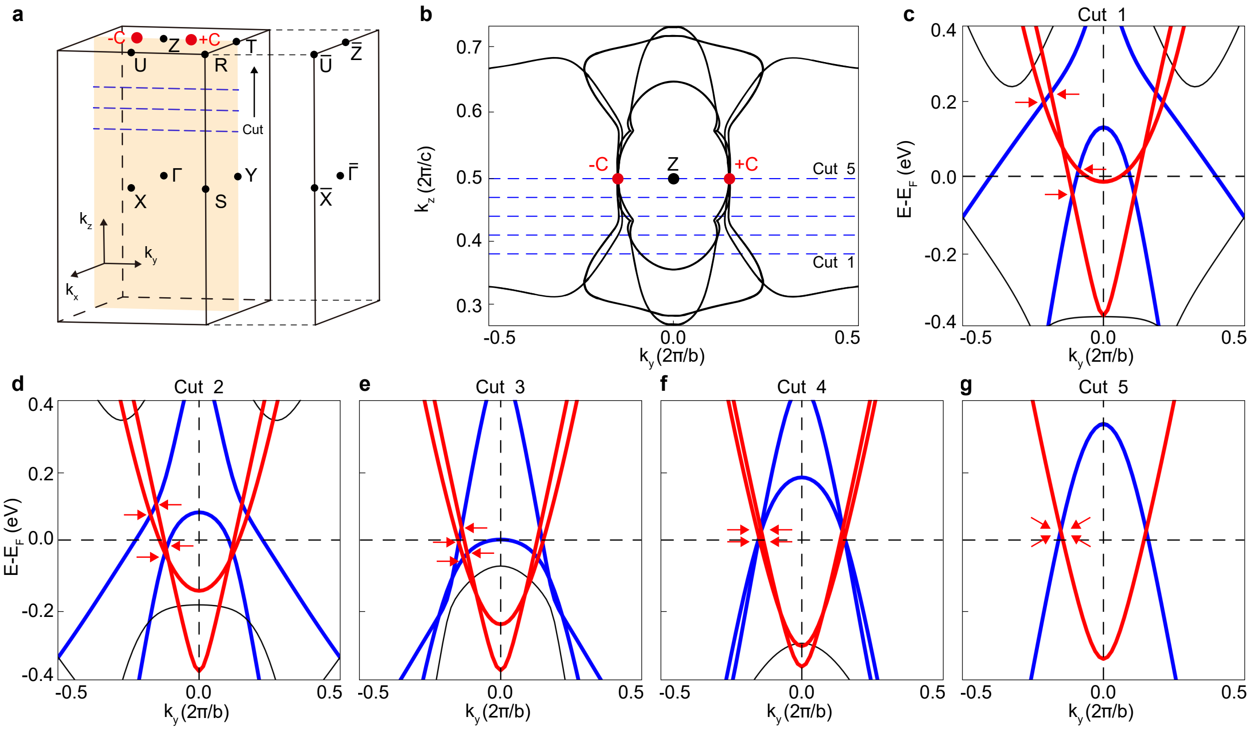

Figure S1: (a) The first Brillouin zone (BZ) of the conventional unit cell and the projected surface Brillouin zone (SBZ). Blue dashed lines mark the cuts on k_y-k_z plane (the yellow shaded area). (b) Calculated nodal lines around the Z point on k_y-k_z plane. Two four-fold degenerate crossing points are labeled as $\pm C$. Five cuts (blue dashed lines) are adopted with different $k_z = 0.38, 0.41, 0.44, 0.47, 0.50$ (in units of $2\pi/c$). (c-g) Band structures along cuts 1 to 5. Cut 5 passes through the Z point. The red arrows indicate the crossing points around the Fermi level. The Fermi levels are set as zero for all plots.

The comparison of the raw data and normalized data

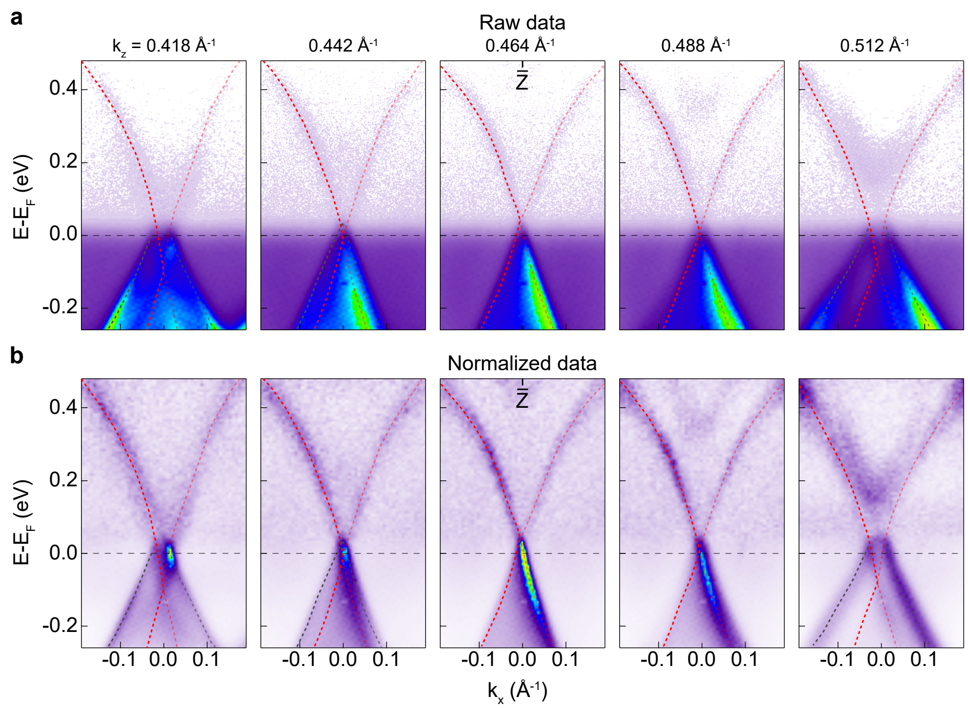

Figure S2: Comparison of the raw data (a) and the normalized data (b).

In order to clearly visualize the dispersion above E_F, the TrARPES dispersion spectra shown in the Figure 1 and Figure 2 in the main text is normalized, in which the intensity at each energy is normalized by the integrated intensity over the full momentum range.[1]

The relaxation of excited electrons in $PtSn_4$

The momentum-dependent fast relaxation of photo-excited electrons observed in our TrARPES measurement results from the electron-phonon (el-ph) interactions, which act as multiple channels for the hot electron relaxation. Under the laser pumping, the electrons below the Fermi level are excited to higher energy bands. Due to electron-electron interactions, these excited electrons are quickly thermalized with a high electron temperature T_e. Then via the el-ph interaction, these hot electrons are relaxed with increasing the lattice temperature T_L. Such relaxation process for hot electrons could be described by the two-temperature (T_e-T_L)

model within the framework of Boltzmann equation[2] and the relaxation rate ($1/\tau$) has the form,

$$\frac{1}{\tau} \sim \left(\frac{\partial F_{k,n}}{\partial t}\right) \sim -\frac{2\pi}{\hbar N_c} \sum_{q,\nu,m} F_{k,n}\left(1 - F_{k+q,m}\right) \lambda_{q\nu nmk}$$
$$= -\frac{2\pi}{\hbar N_c} \sum_{q,\nu,m} F_{k,n}\left(1 - F_{k+q,m}\right) \left|M_{k,n;\,k+q,m}\right|^2 \delta\left(\left|\epsilon_{k+q,m} - \epsilon_{k,n}\right| - \hbar\omega_{q\nu}\right) \tag{1}$$

Herein $M_{k,n;\,k+q,m}$ is el-ph matrix elements, which stands for the initial state with the energy of $\epsilon_{n,k}$ absorbing or emitting a phonon with the energy of $\hbar\omega_{q\nu}$ to the final state ($\epsilon_{m,k+q}$), where n and m label electronic bands, ν is the band index for phonon mode, k (q) is the momentum, $F_{k,n}$ and N_q are the electron and phonon distributions. Starting from the initial state ($\epsilon_{n,k}$), the relaxation of the hot electron is induced by the el-ph collisions, corresponding to the decrease of electron population ($F_{k,n}$). The relaxation rate is faster as the el-ph coupling strength becomes stronger. As shown in Eq. 1, the el-ph relaxation channels also strongly depend on the electronic states around the Fermi level, which act as the final states in the el-ph scattering processes. Thus, the el-ph coupling strength ($\lambda_{q\nu nmk}$) is defined as

$$\lambda_{q\nu nmk} = \left|M_{k,n;\,k+q,m}\right|^2 \delta\left(\left|\epsilon_{k+q,m} - \epsilon_{k,n}\right| - \hbar\omega_{q\nu}\right) \tag{2}$$

On the other hand, as shown in Eq. 1, the relaxation rate in $PtSn_4$ is the sum over all momentum-dependent relaxation time ($1/\tau_{q_i}$), thus we can rewrite the total relaxation time in following, which depends on all parallel channels.

$$\frac{1}{\tau} = \frac{1}{\tau_{q_1}} + \frac{1}{\tau_{q_2}} + \frac{1}{\tau_{q_3}} + \cdots \tag{3}$$

in which each term stands for an el-ph scattering channel with the coupling strength (λ_{q_i}).

In our TrARPES experiment, the sample is cleaved on the (010) surface of $PtSn_4$ in the conventional unit cell, however, we calculate the el-ph coupling matrix in the primitive unit cell. We need to change the conventional unit cell to the primitive unit cell and identify how the momentum points in the conventional BZ connect with those points in the primitive BZ.

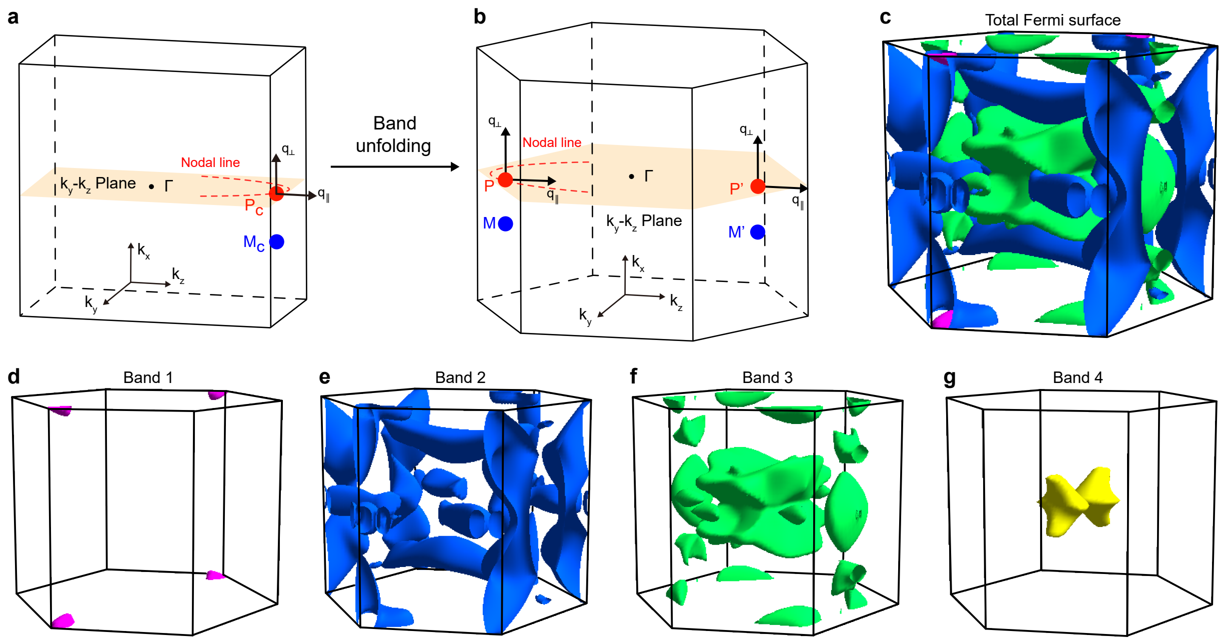

Figure S3: (a) The first Brillouin zone (conventional BZ) of the conventional unit cell for $PtSn_4$. P_c is a crossing point with the fractional coordinate (0.000, 0.148, 0.478) in units of reciprocal vectors in the Dirac nodal line. $q_\perp$ and $q_\parallel$ represent directions perpendicular and parallel to Dirac nodal lines around the P_c point. M_c (-0.100, 0.148, 0.478) is a momentum point along the direction of $q_\perp$ but away from the P_c point. (b) The first Brillouin zone (primitive BZ) of the primitive unit cell for $PtSn_4$. When changing the conventional unit cell to the primitive unit cell, one momentum point in conventional BZ will unfold to more than one point in primitive BZ. For example, in $PtSn_4$, P_c (M_c) point in conventional BZ is unfolded to the P (M) and P′ (M′) points in primitive BZ via the translation vectors G_1=(0, 0, -1) and G_2=(0, 0, 0), respectively. G_1 and G_2 are reciprocal vectors of the conventional BZ. In the primitive BZ, the Dirac nodal line only passes through the P point. (c-g) The Fermi surface of $PtSn_4$ in the primitive BZ. Four bands cross the Fermi level contributing to the complex Fermi surface. Band-dependent Fermi surface is shown in (d-g).

Two types of BZs are illustrated in Figure S3a, b. In the following, we take the P_c point with fractional coordinates (0.000, 0.148, 0.478) in the conventional BZ as an example, on which one crossing point of the Dirac nodal line is located. If we keep the crystal orientation consistent and use the primitive unit cell, P_c will be unfolded to two k-point P and P′ in the primitive BZ (Figure S3a, b). In the vicinity of P_c and P points, the nodal line roughly follows the k_z direction. However, in the primitive unit cell, an energy gap can be found at the P′ point (Figure S5b). Thus, in the following, we take the state at P point in the primitive BZ as the initial state to explore the el-ph coupling matrix. Similarly, we can connect M_c point in the convention BZ with M and M′ points in the primitive BZ, herein M_c point is a k-point slightly away from P_c along the k_x direction.

In $PtSn_4$, fast relaxation processes depend on the large el-ph coupling strength and electronic bands around the Fermi level. As shown in Figure S3, we plot the Fermi surface of $PtSn_4$ in the primitive BZ, which is contributed by four bands (Figure S3d-g) and its distribution in BZ is complex. As shown in the main text, these bulk states could act as final states for el-ph scattering, leading to a rather short relaxation time. This result is consistent with our experimental discoveries.

Figure S4b shows the band structure around the Dirac nodal line for $PtSn_4$. Two bands with the linear dispersion along k_x, named as B1 and B2 states, cross each other at the P point in the primitive BZ. In contrast to discussions in the main text, herein we choose the initial state at the M point (Figure S4a, b) away from the crossing to calculate el-ph coupling matrix in intra-band scattering processes, and mapped its value on the phonon dispersion shown in Figure S4c and S4d. Along the $\boldsymbol{q}_\perp$ direction, only optical phonon modes contribute to el-ph scatterings (Figure S4c). But along the $\boldsymbol{q}_\parallel$ direction, both acoustic and optical phonon modes are involved in the scattering of hot electrons (Figure S4d). Inter-band hopping from the B1 state at the M point along $\boldsymbol{q}_\parallel$ and $\boldsymbol{q}_\perp$ directions is forbidden because the energy difference between the initial and the final states is larger than the maximum of phonon energy.

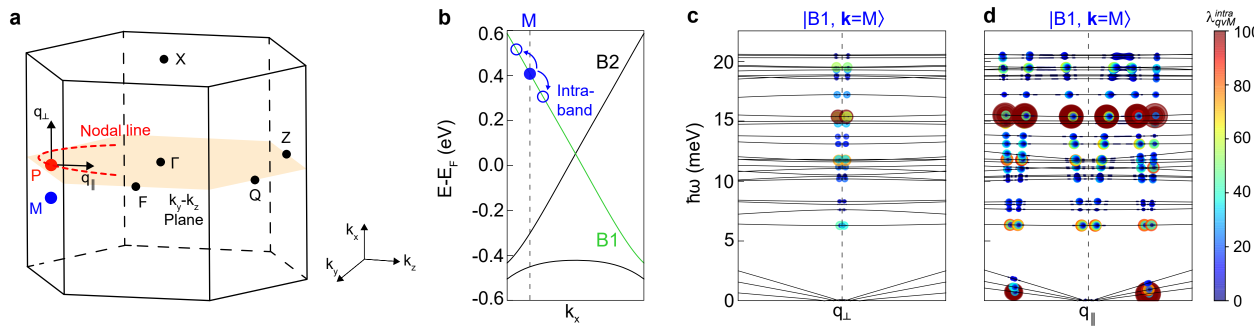

Figure S4: (a) The BZ of the primitive unit cell for $PtSn_4$, $q_\perp$ and $q_\parallel$ are momentum perpendicular and parallel to the Dirac nodal line. (b) The electronic structures around the Dirac nodal line along k_x with two bands crossing each other and labeled as B1 and B2. The Fermi level is set as zero. M point is away from the crossing point. (c, d) Phonon dispersions involving colormaps of el-ph coupling strength for the intra-band hopping. The middle q point corresponds to the Γ point. The el-ph coupling matrix ($\lambda_{q\nu M}^{intra} = \lambda_{q\nu nmM}|_{n=m=B1}$) is mapped on phonon bands, along directions of perpendicular (c) and parallel (d) to the nodal line, which is scattered by different phonon mode initially from B1 state at M point. The size and color of the circles both represent $\lambda_{q\nu k}^{intra}$, q and ν stand for the wave vector and the branch of a phonon mode, respectively.

While, around P′ and M′ points in the primitive BZ (Figure S5a), there is a band gap between B3 and B4 state (Figure S5b). For intra-band scattering processes along the $q_\parallel$ direction, both acoustic and optical phonon modes contribute to the el-ph scattering process, however, along $q_\perp$ direction, acoustic phonon does not contribute to el-ph coupling strength as shown in Figure S5c-f. For inter-band scattering processes, due to the large band gap, only phonon along $q_\parallel$ takes part in the el-ph relaxation from the state of band B4 at the P′ point as shown in Figure S5g-j.

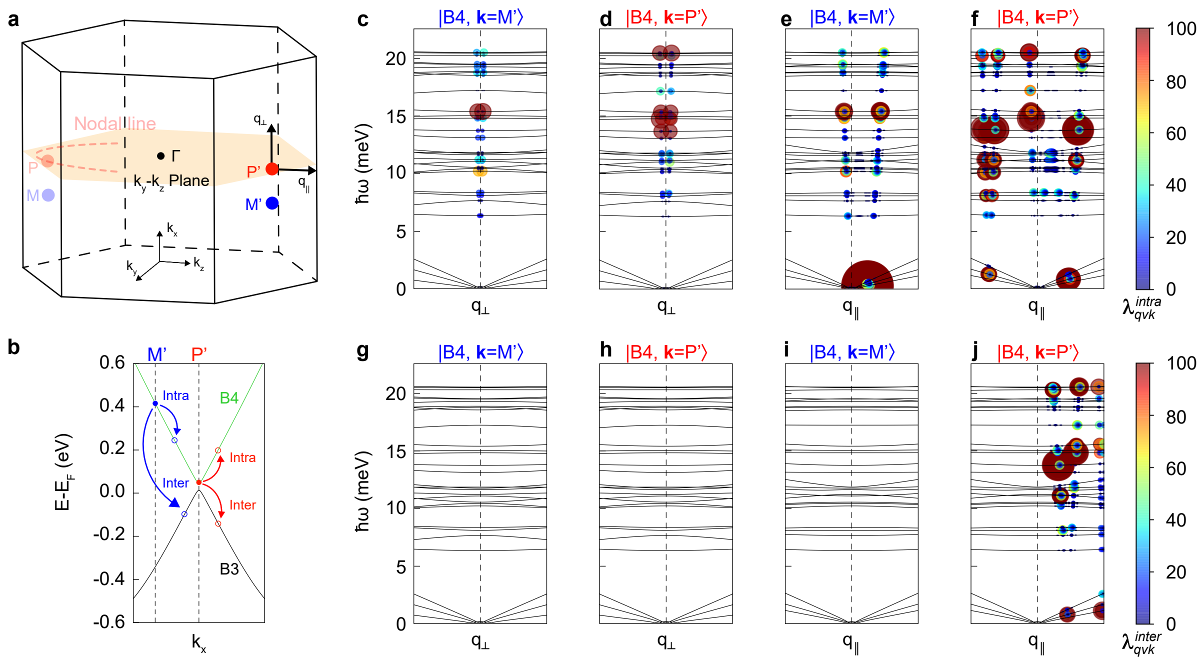

Figure S5: (a) The BZ of the primitive unit cell for $PtSn_4$, $q_\perp$ and $q_\parallel$ have same definitions with those shown in Figure S4. (b) The gapped electronic structures around P′ point. Along k_x two bands are labeled as B3 and B4 with a band gap at the Fermi level, which is set as zero. (c-f) Phonon dispersions involving colormaps of el-ph coupling strength for the intra-band hopping. The middle q point corresponds to the Γ point. The el-ph coupling matrix $\lambda^{intra}_{q\nu M'}$ in (c, e) ($\lambda^{intra}_{q\nu P'}$ in (d, f)) is mapped on phonon bands, which is scattered by different phonon mode for B4 state at the M′ point (at the P′ point). All symbols are defined the same as Figure S4. (g-j) Phonon dispersions involving colormaps of el-ph coupling strength for the inter-band hopping. Along the $q_\parallel$ direction, acoustic phonons with finite q contribute a lot to the el-ph scattering.

The time resolution of the system

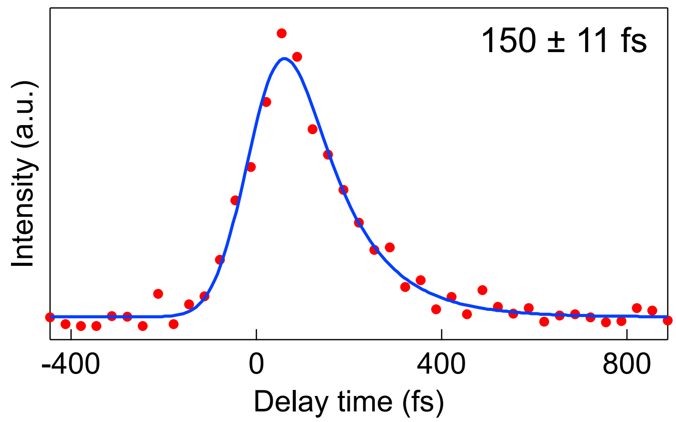

Figure S6: The time resolution extracted from the TrARPES measurement of Sb_2Te_3 by integrating the intensity near the direct excitation.

Influence of spin-orbital coupling effect

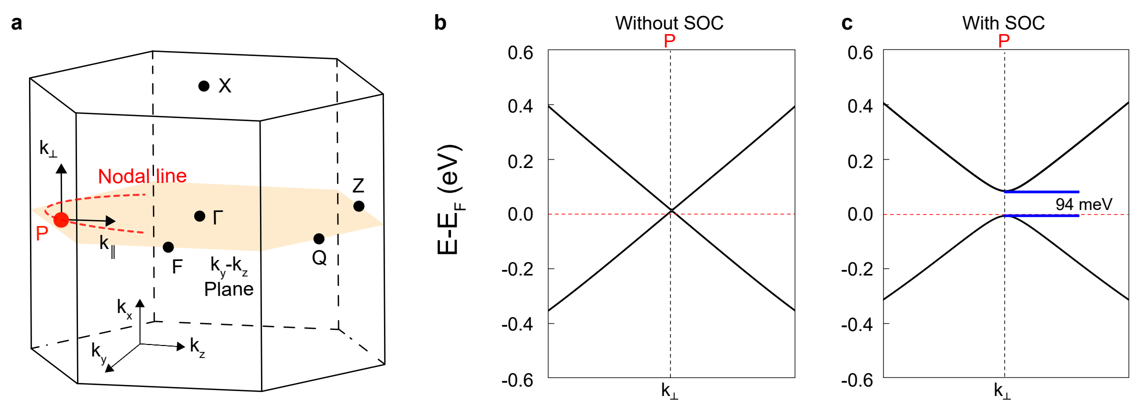

Figure S7: (a) The first Brillouin zone of the primitive cell of $PtSn_4$. P is a crossing point on the nodal line and $k_\perp$ is the momentum direction perpendicular to the nodal line. (b-c) Band structures along $k_\perp$ without SOC (b) and with SOC (c). A band gap of 94 meV will be opened at the P point while the SOC is included in the DFT calculations.

In this part, we discuss the influence of spin-orbit coupling (SOC) effect on the Dirac nodal lines and the related el-ph coupling matrix elements. In bulk $PtSn_4$, the time-reversal symmetry (T) and inversion symmetry (P) are preserved, resulting in the double degeneracy for any bulk state. Correspondingly, no spin textures can be observed on these states neither. When the SOC is considered in our DFT calculations, the finite band gap will be opened at the Dirac nodal lines. Taking the P point (Figure S7a) as an example, the SOC will induce a band gap with the size of 94 meV (Figure S7b-c).

For the el-ph coupling strength, because the SOC term slightly induces a momentum- and band-dependent energy shift on the electronic states around the Dirac nodal lines, the value of el-ph coupling strength will be changed too. While, the spin component of each degenerate states will not affect the el-ph matrix elements.

References

(1) Chang, J.; Shi, M.; Pailhés, S.; Månsson, M.; Claesson, T.; Tjernberg, O.; Bendounan, A.; Sassa, Y.; Patthey, L.; Momono, N.; Oda, M.; Ido, M.; Guerrero, S.; Mudry, C.; Mesot, J. Anisotropic quasiparticle scattering rates in slightly underdoped to optimally doped high-temperature $La_{2-x}Sr_xCuO_4$ superconductors. *Phys. Rev. B* **2008**, *78*, 205103.

(2) Allen, P. B. Theory of thermal relaxation of electrons in metals. *Phys. Rev. Lett.* **1987**, *59*, 1460–1463.